Ceramics International 46 (2020) 6672–6681

Contents lists available at ScienceDirect

Ceramics International

journal homepage: www.elsevier.com/locate/ceramint

Comparative study on crack resistance of TiAlN monolithic and Ti/TiAlN multilayer coatings

Jintao Shuai[a,b], Xiao Zuo[a], Zhenyu Wang[a], Peng Guo[a], Beibei Xu[a], Jia Zhou[a], Aiying Wang[a,b,c,**], Peiling Ke[a,b,c,*]

[a] Key Laboratory of Marine Materials and Related Technologies, Zhejiang Key Laboratory of Marine Materials and Protective Technologies, Ningbo Institute of Materials Technology and Engineering, Chinese Academy of Sciences, Ningbo, 315201, China
[b] Center of Materials Science and Optoelectronics Engineering, University of Chinese Academy of Sciences, Beijing, 100049, China
[c] Ningbo Institute of Industrial Technology, Ningbo, 315201, China

ARTICLE INFO

Keywords:
TiAlN
Multilayer coating
Nanoindentation
Scratch test
Crack resistance
Failure mechanism

ABSTRACT

TiAlN monolithic and Ti/TiAlN multilayer coatings were fabricated on Ti–6Al–4V substrates by a self-designed multisource cathodic arc ion deposition system. The mechanical properties and crack evolution of the coatings were focused under scratch tests with different constant loads. Results showed that the multilayer coating exhibited a higher combination of plasticity, crack resistance and load capacity comparing to those of the monolithic coating. Namely, radical cracks, chippings, and lateral cracks were observed in the monolithic coating after scratch test, whereas only radical cracks occurred in the multilayer coating. The surface and cross-sectional morphology of the scratch tracks revealed that bending and shear stress were responsible for the failure of the two coatings. In particular, the ductile Ti layers within the multilayer coatings could coordinate the deformation and enhance the adhesion between the substrate and the brittle TiAlN layers, which further hindered the propagation of cracks, resulting in a higher crack resistance.

1. Introduction

Hard ceramic coatings, like TiN and TiAlN, have been widely applied in industry because of their high hardness, excellent oxidation resistance and wear resistance [1–5]. With the utilization of hard ceramic coatings, workpieces can be used under aggressive and hash conditions such as aero-engines. However, monolithic ceramic coatings are generally brittle, which results in poor adhesion to substrates and lower crack resistance. In addition, the fracture of brittle coatings can also cause the micro-cracking of the underlying ductile metal substrates, threatening the safety and reliability of engineering structures [6,7]. Those disadvantages frequently lead to unpredictable and catastrophic failure [8,9]. In general, the through-thickness cracks in the ceramic coatings are key factors for the failure of the components, which will allow oxygen and corrosive media to penetrate easily from surface to the metal substrates, causing severe oxidation and corrosion [10–13]. Consequently, the reliability and durability of coatings can be substantially reduced due to the generation of the cracks under service. To obtain long-life hard ceramic coatings, multilayer architecture is one of promising strategy, since it can effectively hinder the propagation of the through-thickness cracks by inducing a large number of interfaces. In this viewpoint, the failure mechanism of wear or erosion changes from single-stage (monolithic coatings) to multi-stage (multilayer coatings). In addition, multilayer coatings, particularly with the alternating layers of materials with different properties, e.g., ductile metals and hard ceramics, exhibit an outstanding property of high hardness, fracture toughness and excellent crack resistance [14–18]. TiAlN has been widely employed as a protective coating due to its high hardness and high resistance to oxidation. But one of its major defects is poor resistance to brittle fracture. With the purpose of improving the toughness of the TiAlN coatings, the multilayer structure coatings composed of the alternative ductile metal and hard ceramics layers have been suggested and investigated by the coating communities. Typically, Ti/TiAlN multilayer coatings exhibit comprehensive performances like high hardness, excellent wear resistance, and high-temperature stability. The multilayer architecture can also endow Ti/TiAlN coating with excellent resistance to wear and erosion, high crack resistance, and fracture toughness and low residual stress, which makes the Ti/TiAlN coatings have great potential in a variety of industrial applications like machining tools, dies and engineering components

* Corresponding author. Ningbo Institute of Industrial Technology, Ningbo, 315201, China.
** Corresponding author. Ningbo Institute of Industrial Technology, Ningbo, 315201, China.
E-mail addresses: aywang@nimte.ac.cn (A. Wang), kepl@nimte.ac.cn (P. Ke).

https://doi.org/10.1016/j.ceramint.2019.11.155
Received 20 September 2019; Received in revised form 26 October 2019; Accepted 19 November 2019
Available online 20 November 2019

[14,19,20].

But for many harsh working conditions, such as erosion of turbine blades, it is still necessary to develop multilayer coatings with a higher crack resistance and fracture toughness. At more fundamental levels, many researchers have reported on crack behaviors within coatings under external load and tried to understand the underlying failure mechanism. For example, Vereschaka et al. [21,22] studied cracking mechanisms in a series of multilayered composite nanostructured coatings during scratch and cutting tests, exploring the balance among the basic properties (hardness, resistance to brittle fracture, internal stress, etc.) of the coatings to achieve high wear resistance and maximum tool life. Wieciński et al. [23] investigated the failure mechanism of Cr/CrN multilayer coatings with different thickness ratios of Cr and CrN layers during indentation. Bigelow and Shen [24] studied the induced shear bend in Al/SiC multilayer coatings by indentation, it was found that strain-softening of the hard layers after yielding was a key factor in shear band formation in thin-film multilayers. Peng et al. [25] demonstrated the damage resistance of sandwich-structured TiN/graded TiSiN/TiSiN film using nanoindentation as well, revealing stress distribution and crack evolution during the loading and unloading.

In general, the crack behavior of coatings was studied under a small and localized load (indentation). There is still a paucity of data concerning the crack behavior under a high and large-scale load (scratching). During the scratch tests, the magnitude of the applied load is much larger than that of the indention, and the stress state of the two tests are quite different, which can significantly change the conditions for crack initiation and propagation. On the other hand, the mechanism of adhesion and crack resistance enhancement by multilayer architecture is still confusing, especially the effect of ductile metal layers in the multilayer coating is still unclear, lacking direct evidence from the detailed and delicate characterization. In order to further improve load capacity and adhesion of the multilayer coatings, it is essential to figure out the failure mechanism of the coatings under scratch tests.

In this study, both TiAlN monolithic and Ti/TiAlN multilayer coatings were deposited on the Ti–6Al–4V titanium alloy substrates. The aim of this work was to comparatively investigate the crack resistance and failure mechanism of the above two coatings during the scratch tests. Particularly, the effect of the ductile metal layers on the crack resistance and adhesion and related failure mechanism was focused in terms of structural evolution. The results here can provide a promising perspective and a better understanding to improve the crack resistance and adhesion by designed multilayer architecture.

2. Experimental

2.1. Coating deposition

The TiAlN monolithic and Ti/TiAlN multilayer coatings for this study were deposited by a self-designed multisource cathodic arc ion deposition system, as illustrated in Fig. 1. Ti targets (for the Ti layers and TiN interlayers) with purity of 99.9 wt % and TiAl targets (for the TiAlN layers) in an atomic ratio of 33: 67 were applied as cathodes. The current of the Ti and TiAl cathodes for all following processes was set at 70 A. Ti–6Al–4V titanium alloy (dimensions of 15 mm × 15 mm × 3 mm) was used as substrates, which were ground down to 5000-grit by SiC abrasive papers before the deposition. The distance between the targets and substrates was 15 cm. Before the deposition process, the substrates' surface was ultrasonically cleaned in ethanol for 20 min to remove residual grit and organic contaminates and dried by pure high-pressure nitrogen. The chamber was evacuated to a base pressure lower than 3×10^{-3} Pa, and heated to 300 °C during the vacuum procedure, and kept at 300 ± 10 °C during the whole process. Then the Ar mass flow controller (supplied by argon with purity of 99.999 vol %) was opened to reach a pressure of 0.27 Pa, the substrates were etched by an Ar ion beam source for 30 min with a current of 0.2 A. Meanwhile, a 100 V negative bias was applied on the substrates. Then increasing the Ar mass flow to reach a pressure of 1.6 Pa, activating the substrate by Ti metal bombardment for 8 min with the negative bias of 500 V. Aforementioned cleaning and the following deposition processes were all performed under the continuous rotation of substrate holder to obtain uniform coatings. For TiAlN monolithic coating, the TiN interlayer was deposited on all samples for 8 min, and then the main coating process for TiAlN lasted for 200 min; for Ti/TiAlN multilayer coating, alternated six cycles of Ti (6 min for each layer) and TiAlN (26 min for each layer). The Ti and TiAlN layers were alternately deposited by controlling the gas supply and the arc power of the targets. Pure argon and pure nitrogen were used during the deposition of Ti layers and TiAlN layers, respectively. The power for the deposition of the Ti and TiAlN layers was periodically turned on and off to deposit Ti and TiAlN layers. Negative bias voltages during the deposition of the TiN interlayer and the main coating process were 60 V and 80 V, respectively. Ti layers within the Ti/TiAlN coating were prepared with a pressure of 2.7 Pa. TiN interlayers and TiAlN layers were all deposited in pure N_2 (supplied by nitrogen with a purity of 99.999 vol %) with the chamber pressure of 6.7 Pa. Detailed parameters of cleaning and deposition processes are shown in Table 1.

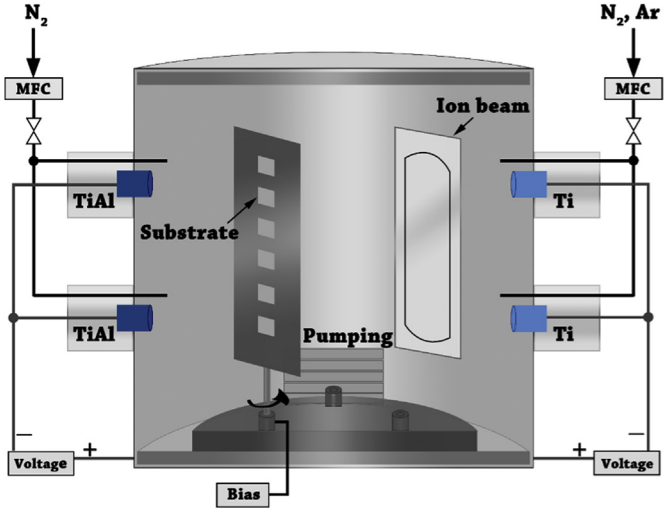

Fig. 1. Schematic diagram of the coating deposition system.

2.2. Scratch tests

Scratch tests were performed using CSM Revetest (Switzerland) equipped with a diamond Rockwell conical indenter (apex angle of 120° and curvature radius of 200 μm) under constant load mode. The scratch tests were conducted in the following three steps: (1) applying a certain normal load on the indenter, (2) scratching the surface of the sample at the speed of 1.5 mm/min for 3 mm with the constant load, (3) unloading. The constant loads for this study varied from 10 N to 80 N, with force interval 10 N. At least three tests for each load were conducted on each sample to acquire solid results, and typical examples with certain loads were selected to analyze.

During scratch tests, acoustic emission (AE) signals were collected and used to analyze the evolution of cracks in the coatings. Acoustic emission describes the emission of the elastic waves caused by the internal energy-releasing during permanent damage in materials. AE accompanies the initiation and propagation of cracks in brittle materials [26].

2.3. Nanoindentation tests

The hardness and elastic modulus of the deposited coatings were determined using nanoindentation (NanoIndentation G200, MTS, USA) with a Berkovich-diamond tip in continuous stiffness measurement

Table 1
Processing parameters of the TiAlN monolithic and Ti/TiAlN multilayer coatings.

Procedure	Pressure (Pa)		Current (A)			Negative bias (V)
	Ar	N_2	Ion beam	Ti cathodes	TiAl cathodes	
Ion cleaning	0.27	–	0.2	–	–	100
Ti bombardment	1.6	–	–	70	–	500
TiN interlayer	–	6.7	–	70	–	60
Ti layer	2.7	0	–	70	–	80
TiAlN layer	–	6.7	–	–	70	80

(CSM), and the applied loads were set at 85 mN and 650 mN for both samples. A Poisson's ratio of 0.25 was assumed for both coatings [27]. To avoid the influence of metallic macroparticles of the coatings and obtain reliable date, samples were polished by ball-cratering apparatus with a 2-cm-radius steel ball for a few seconds before the tests. Twelve random indents were performed on each sample. The values of hardness and elastic modulus were calculated following the model of Oliver and Pharr [28].

2.4. Morphology characterization

Scanning electron microscopy (SEM, FEI Quanta FEG 250) was applied to observe the surface and cross-sectional morphology of the scratch tracks, and the chemical composition of the coatings was determined with the energy-dispersive X-ray spectroscopy (EDS) at an accelerating voltage of 20 kV.

The cross-sectional samples of scratch tracks were cut by a low-speed saw (IsoMetTM, Buehler, USA), then polished by a broad ion beam system (BIB), using Leica EM TIX 3X at voltage of 7 kV, fundamental of BIB technique can be found in Ref. [29].

3. Results and discussion

3.1. Morphology and chemical composition

The cross-sectional micrographs of the TiAlN monolithic coating and the Ti/TiAlN multilayer coating are shown in Fig. 2a–c, respectively. The total thicknesses of the TiAlN monolithic and Ti/TiAlN multilayer coatings were close, about 10.7 μm and 11.5 μm, respectively, including a TiN interlayer with the thickness of ~0.7 μm for both coatings. A small amount of metallic macroparticles, which are commonly incorporated in coatings prepared by cathodic arc deposition, were observed as well. Except for the TiN interlayer, the Ti/TiAlN multilayer coating composed of 12 layers, including 6 TiAlN layers (darker layers in Fig. 2c) alternated with 6 Ti layers (brighter layers in Fig. 2c). The thicknesses of each Ti and TiAlN layer were ~0.4 μm and ~1.4 μm, respectively.

The chemical composition of the TiAlN monolithic coating (spectrum 1 in Fig. 2a) and TiN interlayer (spectrum 2 in Fig. 2a) determined by EDS was shown in Fig. 2b–e, respectively. The EDS line scanning of the Ti/TiAlN multilayer coating revealed the well-defined compositional modulation consisting of alternate brighter Ti layers and darker TiAlN layers (Fig. 2d). The Ti, Al, N and C elements were detected from the EDS, and it should be noted that the N concentration was just around 27 at. % for the TiAlN layer and TiN interlayer. Two main reasons should be considered for the underestimation of nitrogen concentration: (1) weak sensitivity in detecting light elements, like nitrogen [30], is one of the shortcomings of the EDS technique and (2) the overlapping of the $N_{K\alpha}$ and $Ti_{K\beta}$ lines of nitrogen and titanium, respectively [31]. In addition, the concentration of carbon was neglected owing to its low content (lower than 5 at. %) and irrelevance for this study, although it was detectable.

3.2. Mechanical properties

Typical load-depth curves at the loads of 85 and 650 mN for both coatings are presented in Fig. 3a–b. The curves were smooth at both loads for the two coatings, and no pop-in and pop-out events were observed, indicating a good crack resistance and adhesion of the coatings to substrates under indentation [23,32].

Penetration depth of indentation has a strong influence on the determination of hardness. Usually, the contribution of the substrate to the hardness measurements can be neglected when the penetration depth is lower than 10% of the coating thickness [25]. As presented in Fig. 3a, at 85 mN, the penetration depths were ~440 and ~500 nm, corresponding to the TiAlN monolithic coating and the Ti/TiAlN multilayer coating, respectively, which were much lower than 10% of the coating thicknesses. The hardness-depth curves at 85 mN are presented in Fig. 3c. Within the penetration depth of 0–100 nm, the error was large due to the indentation size effect [33], so data was not presented in this study. Within the studied range from 100 to 500 nm, the hardness of the TiAlN monolithic coating slowly decreased with increasing the penetration depth to 100–180 nm, and stabilized at around 35 GPa with penetration depth 180–450 nm. Different from TiAlN monolithic coating, the hardness-depth curve of the Ti/TiAlN multilayer coating can be divided into two stages: (1) the steady stage is between the depth of 100–160 nm, (2) the decline stage is within the range of 160–460 nm. At the steady stage, the hardness of the Ti/TiAlN coating stabilized at around 30 GPa, yet gradually reduced to about 19 GPa at the decline stage. This variation of the Ti/TiAlN multilayer coating hardness can be explained from the influence of the substrate. Assuming the first two layers (one TiAlN layer and one Ti layer) from top of the Ti/TiAlN multilayer coating as a coating-substrate system, the thickness of the TiAlN coating was approximately 1.4 μm, and the penetration depth of 160 nm was roughly corresponding to 10% of the coating thickness under this condition, therefore, the hardness measurements were affected by the Ti layer. As to their elastic modulus, within the range of 100 nm–500 nm, the elastic modulus of both coatings decreased steadily with the increase of displacement into surface, as shown in Fig. 3d, which can also be explained from the effect of the soft substrate, since the substrate effect is unavoidable for the measurements of elastic modulus, due to the long-range elastic field underneath the indenter, even the traditional 10% rule does not strictly apply for nanoindentation measurements for elastic modulus determination of thin-film system [34].

Plastic deformation, leading to stress relaxation in materials, can substantially absorb the energy during deformation and hinder the propagation of cracks. It has been assumed to predict fracture toughness of coatings [35]. Plasticity is defined as the ratio of the plastic displacement over the total displacement in the load-depth curve (Plasticity $= \frac{\varepsilon_p}{\varepsilon}$, where ε_p is the plastic deformation, and ε is the total deformation). The plasticity for both coatings under 85 mN was close, 0.57 and 0.62 corresponding to the TiAlN monolithic and Ti/TiAlN multilayer coatings, respectively. At higher load of 650 mN, the plasticity of the TiAlN monolithic coating kept stable at around 0.58, while the plasticity of the Ti/TiAlN multilayer coating increased evidently to 0.75, due to the high plasticity of the Ti layers, indicating that the

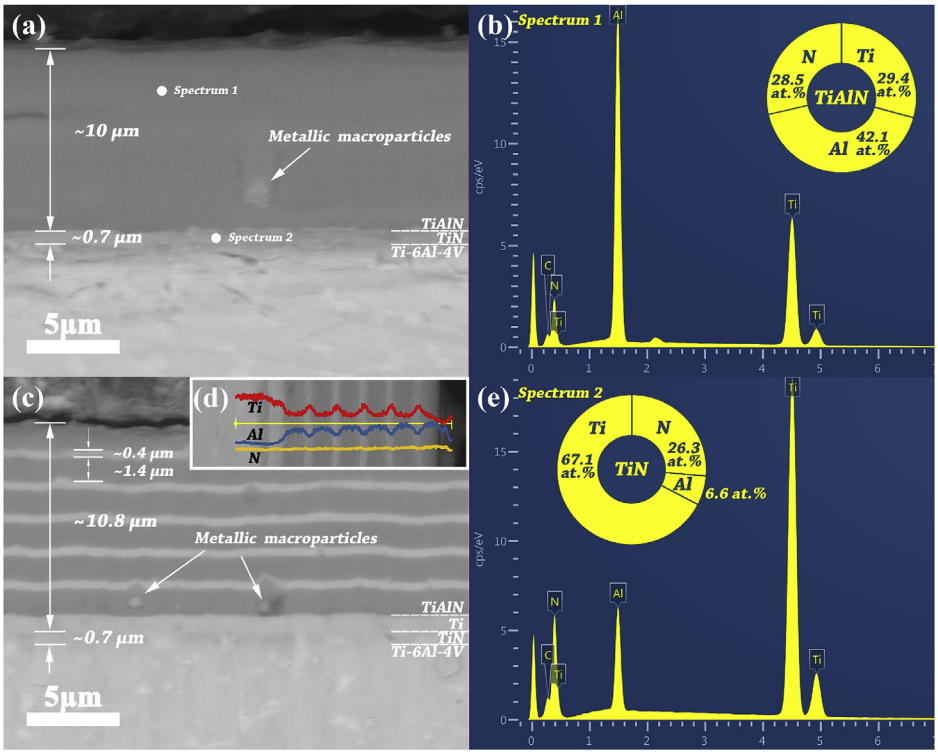

Fig. 2. SEM cross-sectional images of a) the TiAlN monolithic coating and c) the Ti/TiAlN multilayer coating; chemical composition of b) the TiAlN layer and e) the TiN interlayer, corresponding to the spectrum 1 and 2 in Fig. 2a, respectively; d) the cross-sectional EDS line scanning of the Ti/TiAlN multilayer coating.

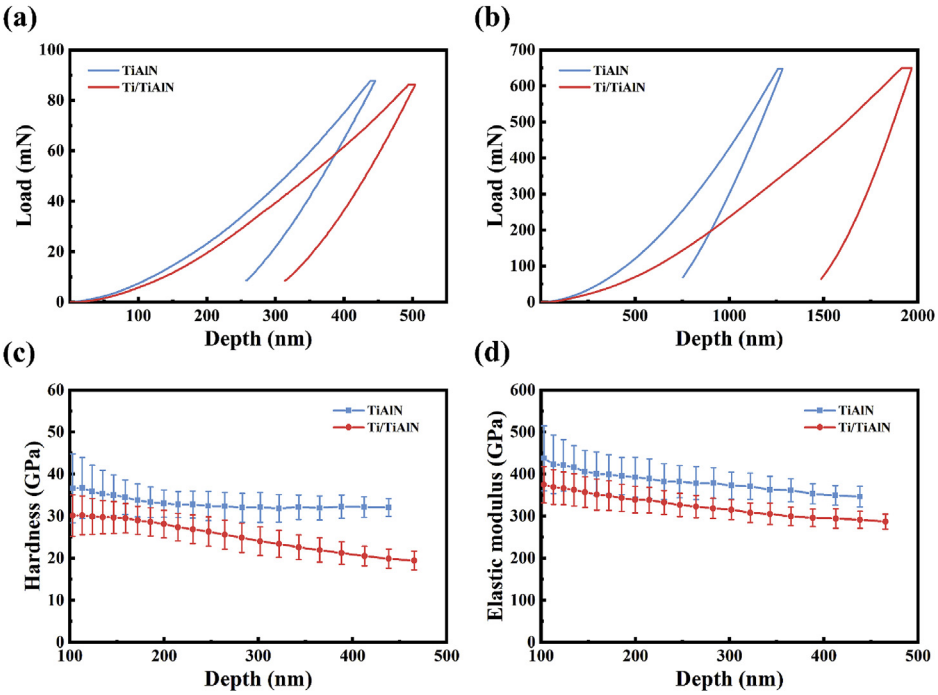

Fig. 3. Indentation curves of the TiAlN monolithic and Ti/TiAlN multilayer coatings at a) 85 mN and b) 650 mN; c) hardness and d) elastic modulus of the TiAlN monolithic coating and the Ti/TiAlN multilayer coating at the maximum load of 85 mN.

metal-ceramics multilayer coatings possessed a better stress relaxation ability than the monolithic ceramic coatings, especially for higher applied load.

3.3. Scratch test

SEM images of scratch tracks of the two coatings at different constant loads are presented in Fig. 4. For the TiAlN monolithic coating, at 10 N (Fig. 4a), no cracks and chippings were observed at the edge and inside of the scratch track, while a narrow and shallow plastic deformation formed; at 30 N (Fig. 4b), tensile macrocracks appeared inside the track, which are typical features when scratching hard coatings on soft substrates, resulting from normal tensile stress and friction force [36,37]. At the edge of the track, some cohesive chippings

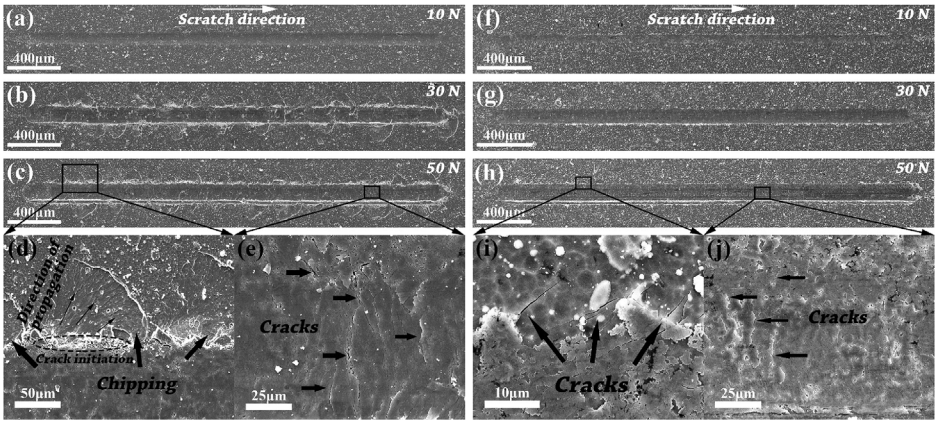

Fig. 4. SEM images of surface morphology of the TiAlN monolithic coating scratched at the constant loads of a) 10 N, b) 30 N and c) 50 N; d) and e) the enlarged images of the framed areas in Fig. 4c; SEM images of surface morphology of the Ti/TiAlN multilayer coating scratched at the constant loads of f) 10 N, g) 30 N and h) 50 N; i) and j) the enlarged images of the framed areas in Fig. 4h.

can be detected, which can be attributed to its poor fracture toughness; increasing the load up to 50 N, the tensile macrocracks became denser and spread longer, and the number of the chippings also increased (Fig. 4c). From the corresponding enlarged images of the cohesive chippings at the edge of the track and macrocracks in the track (Fig. 4d and e), the chipping areas showed the nature of brittle fracture with river-like-pattern appearance, suggesting that the cracks initiated at the edge of the scratch track and propagated inclined outward of the scratch track.

Distinct from the situation happened in the TiAlN monolithic coating, the scratch morphology of the Ti/TiAlN multilayer coating changed slightly with the variety of loads. At all applied loads (10 N, 30 N and 50 N; Fig. 4f, g and 4h), only small and sparse cracks at the edge of the track could be observed and strictly limited inside the scratch track. No cohesive or adhesive chippings occurred, and the cracks were much shorter and sparser compared to those within the TiAlN monolithic coating. With increasing the load from 30 to 50 N, cracks in the scratch track propagated longer (Fig. 4j), few angular cracks at the edge of the track (Fig. 4i), and some short and discontinuous macrocracks in the scratch track can be found at 50 N (Fig. 4j).

Evidently, Ti/TiAlN multilayer coating exhibited a higher load capacity and an enhanced scratch and crack resistance than those of the TiAlN monolithic coating.

The AE signals of the two coatings at different loads were collected as well to study the crack behaviors (Fig. 5). At 10 N, few weak signals were collected for both coatings, indicating the good integrality of the test samples. With increasing the load to 30 N, Ti/TiAlN multilayer coating showed similar AE rate at 10 N, while several significant AE signals appeared for the TiAlN monolithic coating, suggesting a few cracks emerged and then propagated. At 50 N, a great number of strong signals were acquired for both coatings, indicating that many cracks or chippings occurred. However, the amount and amplitude of AE signals of the TiAlN monolithic coating were much larger and higher than those of the Ti/TiAlN multilayer coating, which corroborated the morphology analysis of the scratch tracks. These results confirmed that the crack resistance of the Ti/TiAlN multilayer coating was higher than that of the TiAlN monolithic coating.

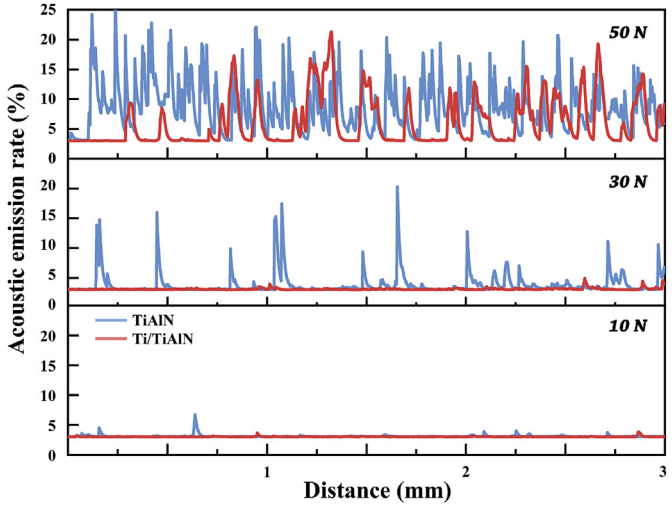

Fig. 5. Acoustic emission rate of the TiAlN monolithic and Ti/TiAlN multilayer coatings during scratch tests at the constant loads of 10 N, 30 N and 50 N.

3.4. Crack resistance and failure mechanism

In order to deeply clarify the crack resistance and the failure mechanism of the coatings during scratch tests, the sectional samples across the direction of the scratch were investigated. To discuss thoroughly and conveniently, the scratch tracks were divided into three parts according to their stress state: (1) beneath the tip of indenter; (2) beneath the face of the indenter; (3) at the edge of scratch tracks, as illustrated in Fig. 6.

Firstly, the cross-sectional micrographs of the scratch tracks of the TiAlN monolithic coating beneath the tip of the indenter are illustrated in Fig. 7. Radical cracks generated at the TiN interlayer and propagated towards the surface at 10 N (Fig. 7a), but the cracks did not penetrate the entire thickness of the coating, indicating that the stress induced by the plastic deformation exceeded the fracture toughness of the coating; at 30 N (Fig. 7b), more radical cracks with larger size appeared in the TiAlN monolithic coating, besides, small lateral cracks also formed. With increasing the load to 50 N (Fig. 7c), both the number and size of lateral cracks became much larger than those at the lower loads. Compared with the cross-sectional morphology under 10 N, 30 N and 50 N, it is easy to find that all radical cracks beneath the tip of the

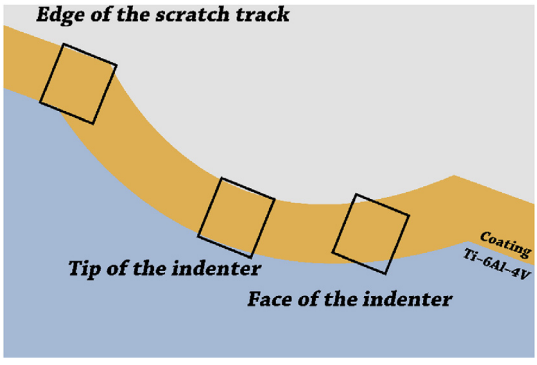

Fig. 6. Schematic diagram of the scratch track.

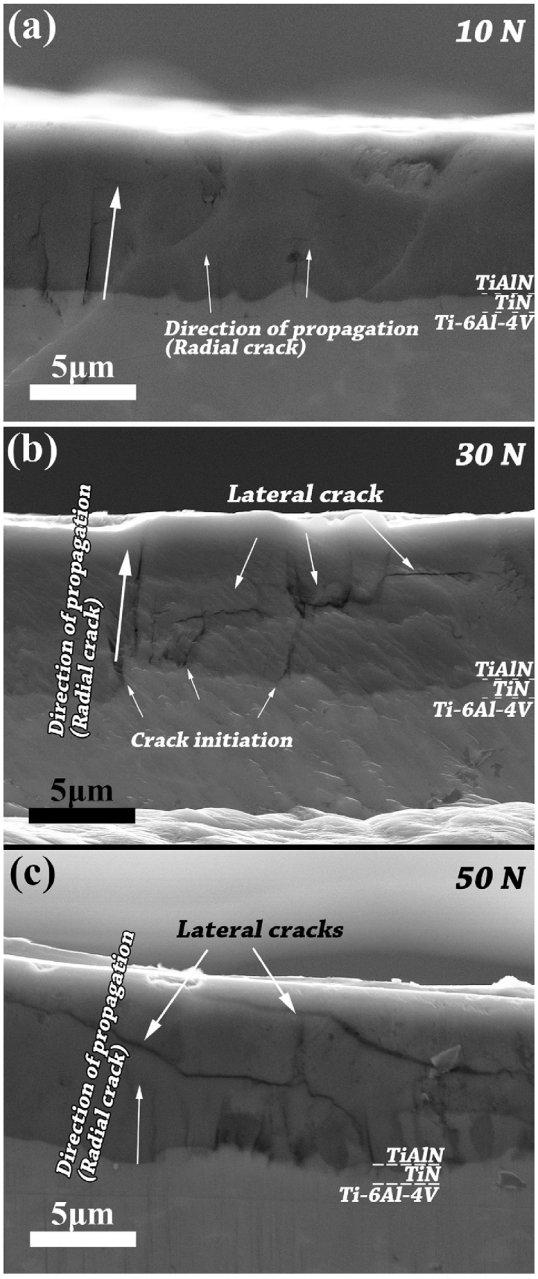

Fig. 7. Cross-sectional SEM images of the TiAlN monolithic coating after scratch tests at the area beneath the tip of indenter at a) 10 N, b) 30 N and c) 50 N.

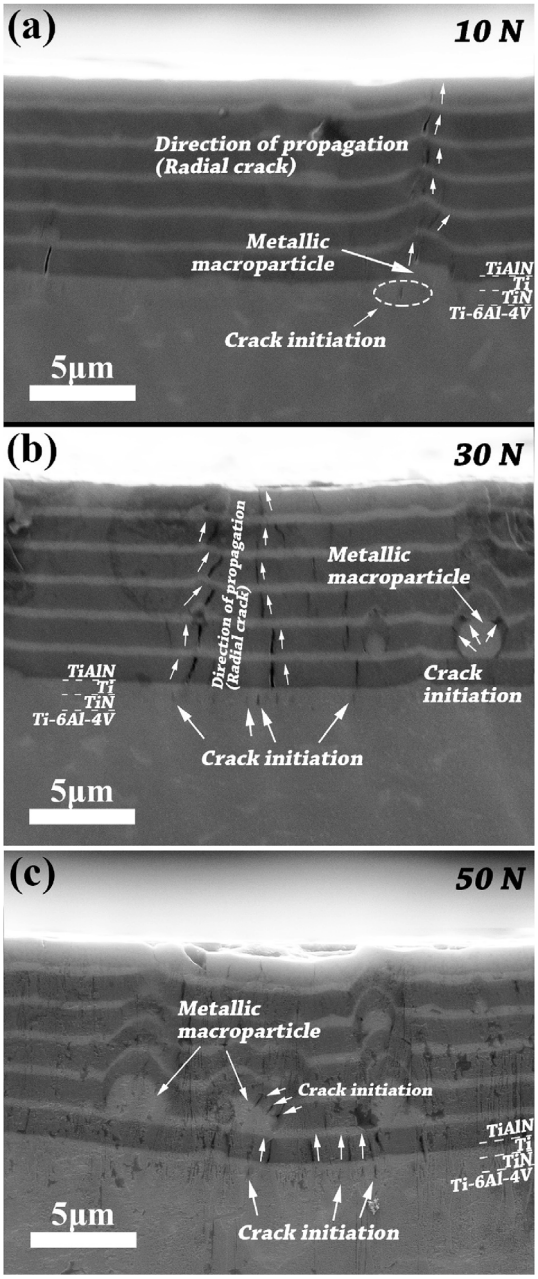

Fig. 8. Cross-sectional SEM images of the Ti/TiAlN multilayer coating after scratch tests at the area beneath the tip of indenter at a) 10 N, b) 30 N and c) 50 N.

indenter spread perpendicularly to the substrate. Under normal applied load, the normal tensile stress can induce deformation of the substrate resulting in bending stress in the coating, which was responsible for the initiation and propagation of the radical cracks [38,39]. In this case, stress states of the upper layer (close to the surface) and the lower layer (close to the substrate) of the coating were different, which corresponded to compressive stress and tensile stress, respectively [40,41]. With increasing applied load from 10 N to 50 N, the plastic deformation enhanced the deformation incoordination of the upper layer and lower layer. Once the plastic deformation exceeded the toughness of TiAlN, consequently, lateral cracks occurred. Moreover, the number of radical cracks increased at 50 N, but the size of them was still small. This phenomenon was probably attributed to: (1) the stress released through either the propagation of large lateral cracks or the increasing number of radical cracks; (2) the growth of radical cracks was blocked by the large lateral cracks (arrowed in Fig. 7c).

Similar to TiAlN monolithic coating, cracks beneath the tip of the indenter initiated at the TiN interlayer within the Ti/TiAlN multilayer coating. Those cracks propagated perpendicularly towards the surface of the coating as well (Fig. 8a). With increasing the applied load from 10 N to 50 N (Fig. 8a, b, and 8c), more and more radical cracks generated in the TiN interlayer due to the bending stress, but no lateral cracks and delamination were observed, even at 50 N. Besides, the cracks were observed only in the TiAlN layers whereas all the Ti layers were free of cracks (Fig. 8). In this case, the deformation induced by the bending stress did not exceed the fracture toughness of the Ti layers, and the cracks generated and were arrested at the interfaces between the TiAlN layers and Ti layers. Different from TiAlN monolithic coatings, TiAlN multilayer coatings had a number of strong interfaces. Apart from that, the ductile Ti layers coordinated the deformation between

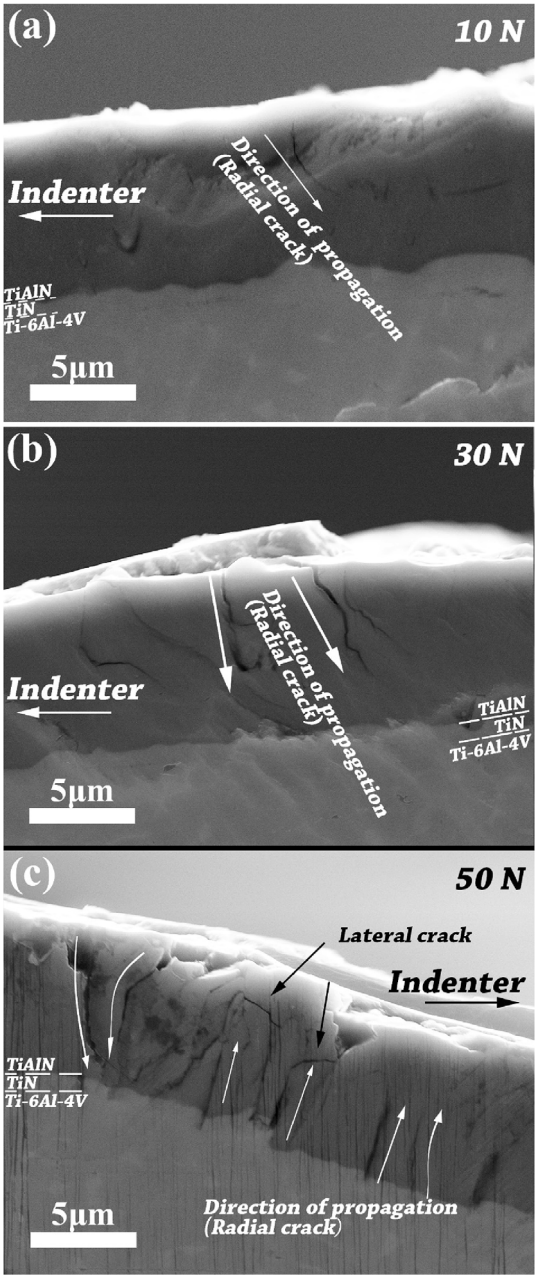

Fig. 9. Cross-sectional SEM images of the TiAlN monolithic coating after scratch tests at the area beneath the face of the indenter at a) 10 N, b) 30 N and c) 50 N.

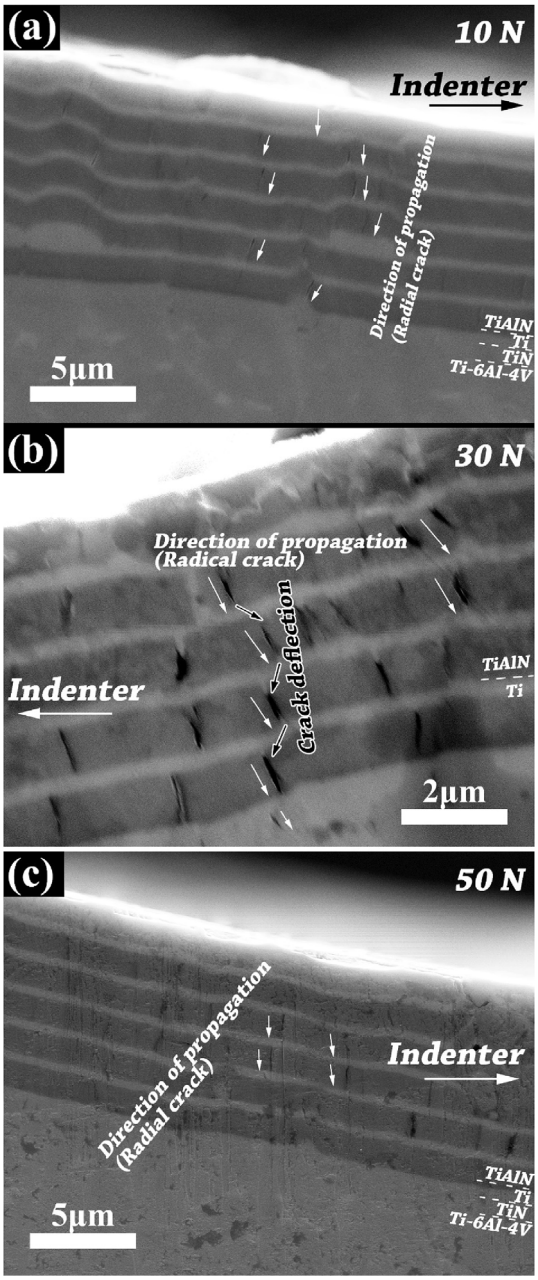

Fig. 10. Cross-sectional SEM images of the Ti/TiAlN multilayer coating after scratch tests at the area beneath the face of the indenter at a) 10 N, b) 30 N and c) 50 N.

the substrate and the TiAlN layers, as well as the different TiAlN layers. The Ti layers behaved like viscous bonding between each hard and brittle TiAlN layers [23]. On the other hand, Ti macroparticles prior to becoming the initiations of radical cracks (Fig. 8b–c), since metallic macroparticles are generally considered as defects in coatings, thus weaken the crack resistance of coatings. Coatings with a better crack resistance should avoid metallic macroparticles of Ti layers as much as possible during the coating deposition.

Secondly, deformation evolution within the TiAlN monolithic coating beneath the face of the indenter was studied from the cross-sectional micrographs (Fig. 9). At 10 N (Fig. 9a), a few radical cracks generated at the surface of the coating and spread towards the substrate. When the load increased to 30 N (Fig. 9b), both the number of radical cracks and their penetration depth increased. And at 10 N and 30 N, the angles between the radical cracks and the substrate were about 45°, indicating that shear stress was the reason that induced the cracks [23,24,38]. At 50 N (Fig. 9c), most of the radical cracks were perpendicular to the substrate, which were similar to the evolution of cracks beneath the tip of the indenter, indicating the lower coating (close to the substrate) was under the normal tensile stress, and the number and size of the radical cracks further grew caused by large plastic deformation of the substrate and the coating under high load; excepting for a few radical cracks generated at the surface and grew towards the substrate, most of the cracks generated at the TiN interlayer and extended perpendicularly towards the surface, since the larger bending stress would cause the fracture of the coating more easily than the shear stress under the large deformation of the substrate; besides, a few small lateral cracks were also found, which was induced by the deflection of the lateral cracks.

Crack evolution beneath the face of the indenter within the Ti/

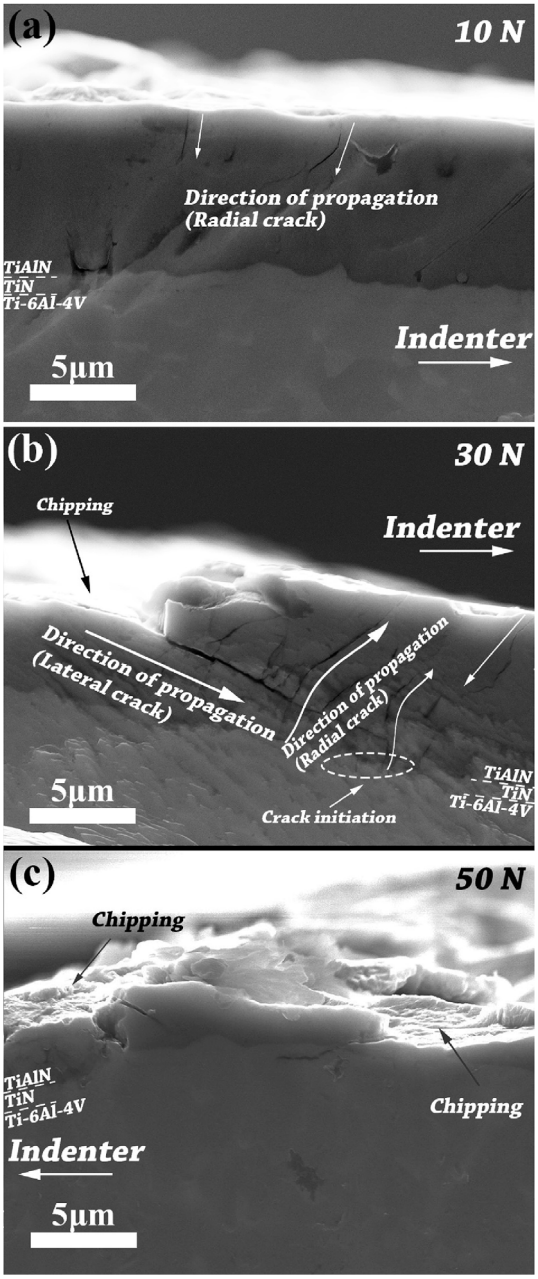

Fig. 11. Cross-sectional SEM images of the TiAlN monolithic coating after scratch tests at the edge of the scratch track at a) 10 N, b) 30 N and c) 50 N.

TiAlN multilayer coating (Fig. 10) was distinct from that within the TiAlN monolithic coating. A few narrow radical cracks initiated at the surface at 10 N (Fig. 10a), and more cracks initiated and spread with increasing the load (Fig. 10b–c). But all cracks extended towards the substrate, and the angles between the cracks and substrate were nearly 90° at all loads. In this case, bending stress was reasonable for the initiation of the cracks rather than the shear stress. But, the direction of bending stress beneath the face of the indenter was opposite to that beneath the tip of the indenter. Radial cracks were still only found in the TiAlN layers, and the crack tips were blunt and hindered at the strong interfaces between Ti layers and TiAlN layers. This was attributed to the fact that the ductile Ti layers absorbed the energy of deformation and accommodated the plastic deformation. The cracks were deflected at the interfaces between Ti layers and TiAlN layers, which was possibly attributed to the difference of the stress distribution in different layers [24]. This phenomenon could avoid stress concentration and improve the crack resistance of the Ti/TiAlN multilayer coating.

In the last step, the crack evolution of the TiAlN monolithic coating at the edge of the scratch tracks can be obtained from Fig. 11. At 10 N (Fig. 11a), small cracks generated at the surface and grew towards the substrate. And the angles between the cracks and the substrate were close to 90°, implying that the tensile stress of the upper coating (close to the surface) was higher than that of the lower coating (close to the substrate), i.e., bending stress caused the break of the coating, which is in good agreement with the previous study [37]. More damages can be observed at 30 N (Fig. 11b), and chippings occurred, suggesting the massive stress induced by a large amount of the plastic deformation exceeded the toughness of the coating, and the propagation of the chippings triggered a long and wide lateral crack. Most of the radical cracks initiated in the TiN interlayer and propagated towards the surface, indicating the bending curvature beneath the tip of the indenter further increased. Combined with the earlier analysis of chippings (section 3.3, Fig. 4c and d), cracks started at the edge of the scratch track, then spread towards not only outside of the track, but also inside of the track (subsurface), which can be mainly explained from the different deformation between the upper layer (close to the surface) and the lower layer (close to the substrate) of the coating. And the area of chippings enlarged with the load increased to 50 N (Fig. 11c).

The failure evolution of the Ti/TiAlN multilayer coating at the edge of the scratch tracks was different from that of the TiAlN monolithic coating, as presented in Fig. 12. Due to the high plasticity and the good deformation coordination, the Ti/TiAlN multilayer coating did not show any defects or cracks at the edge of the scratch track under 10 N, hence the image was not presented. At 30 N, a small number of radical cracks initiated at the top TiAlN layer and spread towards the substrate, but only presented in the TiAlN layers (Fig. 12a). In addition, through-thickness cracks were observed, showing the nature of shear stress.

To further understand the related failure mechanism of the Ti/TiAlN multilayer coating, scratch tests with higher loads (40 N, 60 N and 80 N) were also conducted to the samples. At 40 N, many wide radical cracks existed in TiAlN layers and the Ti layers exhibited great deformation without any cracks, due to the excellent plasticity and ductility of the Ti layers (Fig. 12b), even at 60 N, only deformation and fracture emerged within the Ti/TiAlN multilayer coating (Fig. 12c). Adhesive failure or delamination occurred until the load increased to 80 N (Fig. 12d), and the delamination of the coating was detected. This phenomenon was due to the induced shear and bending stress beyond the tolerance of the bonding strength between the coating and the substrate, as well as the strength between the interfaces. The evolution of the Ti/TiAlN multilayer coating can be explained from the role of the Ti layers and strong interfaces under different loads. In the multilayered architecture, the Ti layer can work as glue, bonding the brittle and hard TiAlN layers, with increasing load, the ductile Ti layers can coordinate the deformation between the substrate and the TiAlN layers and absorb energy due to deformation, and the strong interfaces could hinder the propagation of the cracks in the TiAlN layers, resulting in the high toughness of the Ti/TiAlN multilayer coating, and the possible crack evolution.

In this study, the architecture of the metal-ceramics multilayer coating improved the fracture toughness and crack resistance compared to those of the TiAlN monolithic coating. The presence of the ductile metal layers enhanced the cohesion and adhesion between the coating and the substrate, constrained the deformation of the hard layers and failure mechanism of the Ti/TiAlN coating are proposed, as presented in Fig. 13.

4. Conclusions

TiAlN monolithic and Ti/TiAlN multilayer coatings were deposited on Ti–6Al–4V substrates by a self-designed multisource cathodic arc ion deposition system. The crack resistance and failure mechanism during

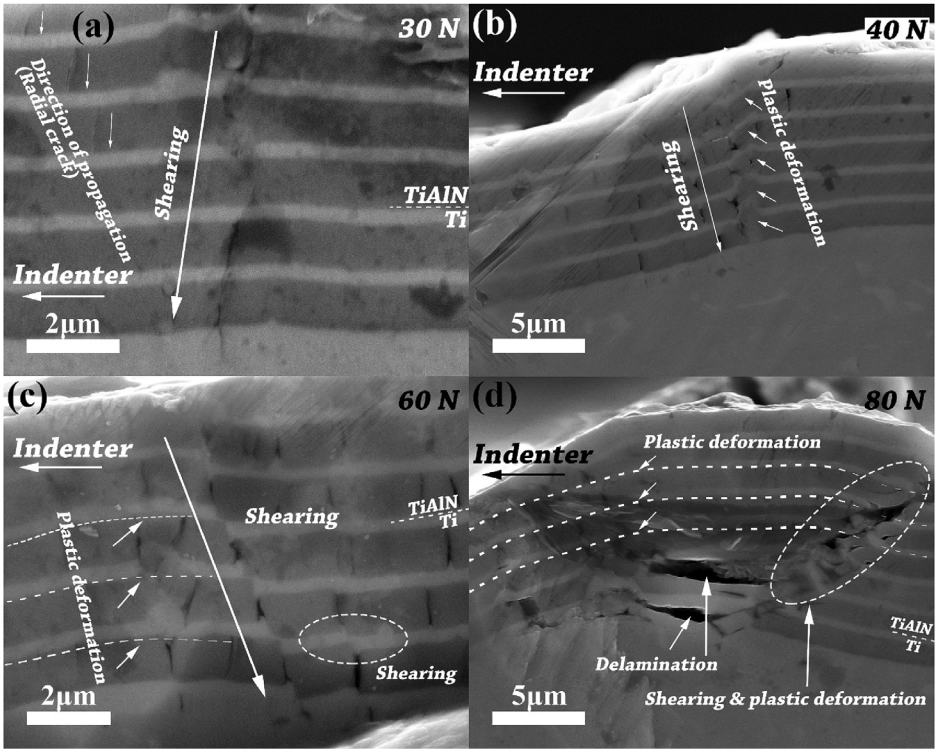

Fig. 12. Cross-sectional SEM images of the Ti/TiAlN multilayer coating after scratch tests at the edge of the scratch track at a) 30 N, b) 40 N, c) 60 N and d) 80 N.

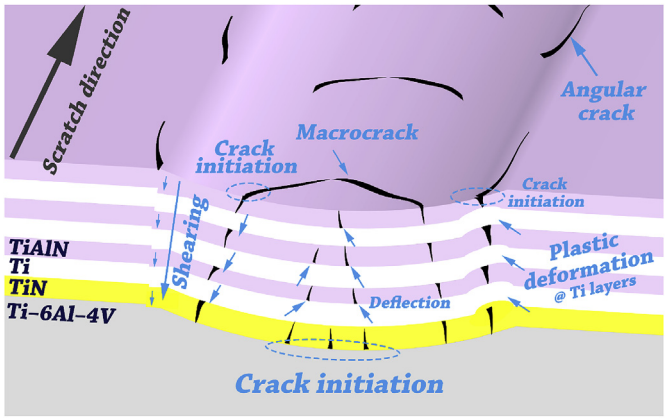

Fig. 13. Schematic illustrations of crack evolution and failure mechanism of the Ti/TiAlN multilayer coating.

scratch tests in terms of structural evolution were investigated. The TiAlN monolithic coating exhibited higher hardness and elastic modulus but lower plasticity and load capacity, comparing to those of the Ti/TiAlN multilayer coating. The ductile Ti layers in Ti/TiAlN system and the formed strong interfaces could coordinate the deformation between the substrate and the TiAlN layers and absorb strain energy due to deformation, which suppressed the propagation of the cracks significantly, resulting in the high toughness of the Ti/TiAlN multilayer coating.

Declaration of competing interests

The authors declare that they have no known competing financial interests or personal relationships that could have appeared to influence the work reported in this paper.

Acknowledgements

The authors are grateful for the financial support from the National Science and Technology Major Project (2017-VII-0012-0108), National Natural Science Foundation of China (51875555, 11705258).

References

[1] K. Yalamanchili, F. Wang, H. Aboulfadl, J. Barrirero, L. Rogström, E. Jiménez-Pique, F. Mücklich, F. Tasnadi, M. Odén, N. Ghafoor, Growth and thermal stability of TiN/ZrAlN: effect of internal interfaces, Acta Mater. 121 (2016) 396–406, https://doi.org/10.1016/j.actamat.2016.07.006.

[2] S. PalDey, S.C. Deevi, Single layer and multilayer wear resistant coatings of (Ti,Al)N: a review, Mater. Sci. Eng., A 342 (1–2) (2003) 58–79, https://doi.org/10.1016/s0921-5093(02)00259-9.

[3] M. Tkadletz, C. Hofer, C. Wüstefeld, N. Schalk, M. Motylenko, D. Rafaja, H. Holzschuh, W. Bürgin, B. Sartory, C. Mitterer, C. Czettl, Thermal stability of nanolamellar fcc-$Ti_{1-x}Al_xN$ grown by chemical vapor deposition, Acta Mater. 174 (2019) 195–205, https://doi.org/10.1016/j.actamat.2019.05.044.

[4] M. Meindlhumer, J. Zalesak, R. Pitonak, J. Todt, B. Sartory, M. Burghammer, A. Stark, N. Schell, R. Daniel, J.F. Keckes, M. Lessiak, A. Kopf, R. Weissenbacher, J. Keckes, Biomimetic hard and tough nanoceramic Ti-Al-N film with self-assembled six-level hierarchy, Nanoscale 11 (16) (2019) 7986–7995, https://doi.org/10.1039/c8nr10339a.

[5] R. Daniel, M. Meindlhumer, W. Baumegger, J. Todt, J. Zalesak, T. Ziegelwanger, C. Mitterer, J. Keckes, Anisotropy of fracture toughness in nanostructured ceramics controlled by grain boundary design, Mater. Des. 161 (2019) 80–85, https://doi.org/10.1016/j.matdes.2018.11.028.

[6] T. Guo, Y. Chen, R. Cao, X. Pang, J. He, L. Qiao, Cleavage cracking of ductile-metal substrates induced by brittle coating fracture, Acta Mater. 152 (2018) 77–85, https://doi.org/10.1016/j.actamat.2018.04.017.

[7] T. Guo, L. Qiao, X. Pang, A.A. Volinsky, Brittle film-induced cracking of ductile substrates, Acta Mater. 99 (2015) 273–280, https://doi.org/10.1016/j.actamat.2015.07.059.

[8] R.O. Ritchie, The conflicts between strength and toughness, Nat. Mater. 10 (11) (2011) 817–822, https://doi.org/10.1038/nmat3115.

[9] S. Kumar, W.A. Curtin, Crack interaction with microstructure, Mater. Today 10 (9) (2007) 34–44, https://doi.org/10.1016/S1369-7021(07)70207-9.

[10] W. Dai, Q. Wang, K.-H. Kim, S.-H. Kwon, Al_2O_3/CrAlSiN multilayer coating deposited using hybrid magnetron sputtering and atomic layer deposition, Ceram. Int. 45 (9) (2019) 11335–11341, https://doi.org/10.1016/j.ceramint.2019.02.211.

[11] G. Li, L. Li, M. Han, S. Luo, J. Jin, L. Wang, J. Gu, H. Miao, The performance of TiAlSiN coated cemented carbide tools enhanced by inserting Ti interlayers, Metals 9 (9) (2019) 918.

[12] G.M. Song, Y.T. Pei, W.G. Sloof, S.B. Li, J.T.M. De Hosson, S. van der Zwaag, Oxidation-induced crack healing in Ti_3AlC_2 ceramics, Scr. Mater. 58 (1) (2008) 13–16, https://doi.org/10.1016/j.scriptamat.2007.09.006.
[13] M. Zhang, F. Zhou, Q. Wang, Y. Fu, Z. Zhou, Structural and tribological properties of CrMoCN coatings with various Mo contents in artificial seawater, Appl. Surf. Sci. 493 (2019) 485–496, https://doi.org/10.1016/j.apsusc.2019.06.297.
[14] E. Vogli, W. Tillmann, U. Selvadurai-Lassl, G. Fischer, J. Herper, Influence of Ti/TiAlN-multilayer designs on their residual stresses and mechanical properties, Appl. Surf. Sci. 257 (20) (2011) 8550–8557, https://doi.org/10.1016/j.apsusc.2011.05.013.
[15] K.S. Selivanov, A.M. Smyslov, Y.M. Dyblenko, I.P. Semenova, Erosive wear behavior of Ti/Ti(V,Zr)N multilayered PVD coatings for Ti–6Al–4V alloy, Wear 418 (2019) 160–166, https://doi.org/10.1016/j.wear.2018.11.016.
[16] F. Bouville, E. Maire, S. Meille, B. Van de Moortele, A.J. Stevenson, S. Deville, Strong, tough and stiff bioinspired ceramics from brittle constituents, Nat. Mater. 13 (5) (2014) 508–514, https://doi.org/10.1038/nmat3915.
[17] P. Wieciński, J. Smolik, H. Garbacz, K.J. Kurzydlowski, Microstructure and mechanical properties of nanostructure multilayer CrN/Cr coatings on titanium alloy, Thin Solid Films 519 (12) (2011) 4069–4073, https://doi.org/10.1016/j.tsf.2011.01.183.
[18] P. Wieciński, J. Smolik, H. Garbacz, K.J. Kurzydlowski, Erosion resistance of the nanostructured Cr/CrN multilayer coatings on Ti6Al4V alloy, Vacuum 107 (2014) 277–283, https://doi.org/10.1016/j.vacuum.2014.02.024.
[19] L.A. Dobrzański, K. Lukaszkowicz, A. Križ, Properties of the multi-layer Ti/CrN and Ti/TiAlN coatings deposited with the PVD technique onto the brass substrate, J. Mater. Process. Technol. 143–144 (2003) 832–837, https://doi.org/10.1016/s0924-0136(03)00351-0.
[20] W. Tillmann, E. Vogli, S. Momeni, Mechanical and tribological properties of Ti/TiAlN duplex coatings on high and low alloy tool steels, Vacuum 84 (3) (2009) 387–392, https://doi.org/10.1016/j.vacuum.2009.08.001.
[21] A.A. Vereschaka, S.N. Grigoriev, Study of cracking mechanisms in multi-layered composite nano-structured coatings, Wear 378–379 (2017) 43–57, https://doi.org/10.1016/j.wear.2017.01.101.
[22] A.A. Vereschaka, S.N. Grigoriev, N.N. Sitnikov, A.D. Batako, Delamination and longitudinal cracking in multi-layered composite nano-structured coatings and their influence on cutting tool life, Wear 390–391 (2017) 209–219, https://doi.org/10.1016/j.wear.2017.07.021.
[23] P. Wieciński, J. Smolik, H. Garbacz, K.J. Kurzydłowski, Failure and deformation mechanisms during indentation in nanostructured Cr/CrN multilayer coatings, Surf. Coat. Technol. 240 (2014) 23–31, https://doi.org/10.1016/j.surfcoat.2013.12.006.
[24] S. Bigelow, Y.L. Shen, Indentation-induced shear band formation in thin-film multilayers, Front. Mater. 4 (2017) 4, https://doi.org/10.3389/fmats.2017.00025.
[25] R. Saha, W.D. Nix, Effects of the substrate on the determination of thin film mechanical properties by nanoindentation, Acta Mater. 50 (1) (2002) 23–38, https://doi.org/10.1016/S1359-6454(01)00328-7.
[26] J. Tomastik, R. Ctvrtlik, M. Drab, J. Manak, On the importance of combined scratch/acoustic emission test evaluation: SiC and SiCN thin films case study, Coatings 8 (5) (2018) 15, https://doi.org/10.3390/coatings8050196.
[27] R. Wei, C. Rincon, E. Langa, Q. Yang, Microstructure and tribological performance of nanocomposite Ti–Si–C–N coatings deposited using hexamethyldisilazane precursor, J. Vac. Sci. Technol., A 28 (5) (2010) 1126–1132, https://doi.org/10.1116/1.3463709.
[28] W.C. Oliver, G.M. Pharr, An improved technique for determining hardness and elastic modulus using load and displacement sensing indentation experiments, J. Mater. Res. 7 (6) (2011) 1564–1583, https://doi.org/10.1557/jmr.1992.1564.
[29] R. Jiang, M. Li, Y. Yao, J. Guan, H. Lu, Application of BIB polishing technology in cross-section preparation of porous, layered and powder materials: a review, Front. Mater. Sci. (2019), https://doi.org/10.1007/s11706-019-0457-0.
[30] A.D. Pogrebnjak, V.M. Beresnev, O.V. Bondar, B.O. Postolnyi, K. Zaleski, E. Coy, S. Jurga, M.O. Lisovenko, P. Konarski, L. Rebouta, J.P. Araujo, Superhard CrN/Mon coatings with multilayer architecture, Mater. Des. 153 (2018) 47–59, https://doi.org/10.1016/j.matdes.2018.05.001.
[31] M.W. Reedy, T.J. Eden, J.K. Potter, D.E. Wolfe, Erosion performance and characterization of nanolayer (Ti,Cr)N hard coatings for gas turbine engine compressor blade applications, Surf. Coat. Technol. 206 (2–3) (2011) 464–472, https://doi.org/10.1016/j.surfcoat.2011.07.063.
[32] J. Weng, X. Zuo, L. Liu, Z. Wang, P. Ke, X. Wei, A. Wang, Dense nanocolumnar structure induced anti-corrosion CrB2 coating with (0 0 1) preferred orientation deposited by DC magnetron sputtering, Mater. Lett. 240 (2019) 180–184, https://doi.org/10.1016/j.matlet.2019.01.002.
[33] H. Li, A. Ghosh, Y.H. Han, R.C. Bradt, The frictional component of the indentation size effect in low load microhardness testing, J. Mater. Res. 8 (5) (2011) 1028–1032, https://doi.org/10.1557/jmr.1993.1028.
[34] A.C. Fischer-Cripps, Nanoindentation, third ed., Springer, New York, 2011, https://doi.org/10.1007/978-1-4419-9872-9.
[35] S. Zhang, D. Sun, Y.Q. Fu, H.J. Du, Toughness measurement of thin films: a critical review, Surf. Coat. Technol. 198 (1–3) (2005) 74–84, https://doi.org/10.1016/j.surfcoat.2004.10.021.
[36] A.R. Shugurov, M.S. Kazachenok, Mechanical properties and tribological behavior of magnetron sputtered TiAlN/TiAl multilayer coatings, Surf. Coat. Technol. 353 (2018) 254–262, https://doi.org/10.1016/j.surfcoat.2018.09.001.
[37] Y. Xie, H.M. Hawthorne, Effect of contact geometry on the failure modes of thin coatings in the scratch adhesion test, Surf. Coat. Technol. 155 (2–3) (2002) 121–129, https://doi.org/10.1016/S0257-8972(02)00064-6.
[38] D. Gross, T. Seelig, Fracture Mechanics, third ed., Springer, Cham, 2018, https://doi.org/10.1007/978-3-319-71090-7.
[39] J.Y. Zhang, X. Zhang, R.H. Wang, S.Y. Lei, P. Zhang, J.J. Niu, G. Liu, G.J. Zhang, J. Sun, Length-scale-dependent deformation and fracture behavior of Cu/X (X = Nb, Zr) multilayers: the constraining effects of the ductile phase on the brittle phase, Acta Mater. 59 (19) (2011) 7368–7379, https://doi.org/10.1016/j.actamat.2011.08.016.
[40] C.K.H. Dharan, B.S. Kang, I. Finnie, Finnie's Notes on Fracture Mechanics, Springer, New York, 2016, https://doi.org/10.1007/978-1-4939-2477-6.
[41] A. Azizpour, R. Hahn, F.F. Klimashin, T. Wojcik, E. Poursaeidi, P.H. Mayrhofer, Deformation and cracking mechanism in CrN/TiN multilayer coatings, Coatings 9 (6) (2019) 17, https://doi.org/10.3390/coatings9060363.